Explaining Deep Time Series Classifiers

by

Prathyush S Parvatharaju

A Thesis

Submitted to the Faculty

of the

WORCESTER POLYTECHNIC INSTITUTE

In partial fulfillment of the requirements for the

Degree of Master of Science

in

Data Science

by

December 2021

APPROVED:

Professor Elke A. Rundensteiner, Thesis Advisor

Professor Xiangnan Kong, Thesis Reader

Abstract

Deep neural networks are being used to build autonomous systems that will perceive, learn, decide, and act on their own. However, state-of-the-art deep learning models lack transparency in how they make their predictions. Explainable classification is essential to high-impact settings where practitioners require *evidence* to support their decisions. Various saliency methods have been developed to summarize where the deep neural networks "look" in the provided input as evidence for the predictions.

One increasingly popular solution is attribution-based explainability, which finds the impact of input features on the model's predictions. While these methods are designed for images, while very little has been done to explain deep time series classifiers. Unlike images, where a pixel has a predefined scale and representation i.e, 0 (black) - 255 (white) and the same is followed across all the image datasets, the distribution of timeseries vary vastly amongst datasets. Also, during classification, short contiguous subsequences often contain much of the discriminative information. However, existing explainability methods treat all input features independently, ignoring correlations and possibly disrupting discriminative subsequences.

In this work, we study this problem and propose PERT, a novel perturbation-based explainability method designed to explain deep classifiers' decisions on time series. PERT extends beyond recent perturbation methods to generate a saliency map that assigns importance values to the timesteps of the instance-of-interest.

First, PERT uses Prioritized Replacement Selector to learn to sample a replacement time series from a large dataset, to perform *meaningful* perturbations and avoid creating network artifacts Second, PERT mixes the instance with the replacements using a Guided Perturbation Strategy, which learns to what degree each timestep

can be perturbed without altering the classifier's final prediction. These two steps jointly learn to identify the fewest and most impactful timesteps that explain the classifier's prediction.

We evaluate PERT using three metrics on nine popular datasets with two black-box models - Fully Connected Network and Recurrent Neural Network. The chosen datasets varies from instances having sequence length of 96 to 720. We find that PERT consistently outperforms all five state-of-the-art methods by a margin of *26%*. Using case studies, we also demonstrate that PERT succeeds in finding the relevant regions of the input time series.

Acknowledgements

I have taken efforts in this project. However, it would not have been possible without the kind support and help of many individuals. I would like to extend my sincere thanks to all of them.

I am highly indebted to my professor Dr. Elke A. Rundensteiner for her motivation and support as my Thesis Advisor. Her insights and critical comments on my research have helped channelise my thoughts and energy towards fruitful research. I owe my deep gratitude to Professor Dr. Xiangnan Kong for his generous time spent being my thesis reader. I appreciate the keen interest taken by him in my project and for guiding me within the limited time frame.

I heartily thank Dr. Tom Hartvigsen for guiding me all the way through; right from defining a problem, designing experiments to assisting in writing and articulation. I'm obliged for having received his mentorship till the successful completion of this work. I'm courteous towards Ramesh Doddaiah, Ph.D. candidate at WPI his collaboration.

I am thankful and fortunate enough to get constant support and encouragement from Academic and Research Computing group at Worcester Polytechnic Institute. They supported us with the computational resources. We used Weights Biases [4] for experiment tracking and visualisation.

This research was supported by the U.S. Dept. of Education grant P200A180088, NSF grant 1910880, NSF CSSI: FAIN: 2103832, Oak Ridge Associated Universities CA W911NF-16-2-0008 and W911NF20-2-0232.

Last but not the least, I would like to express my profound gratitude towards my family for their kind co-operation and encouragement throughout my years of study and research, which helped me in the successful completion of this project.

Contents

1 Introduction **1**

1.1 Background . . . 1

1.2 Motivating Example . . . 2

1.3 State-of-the-Art . . . 3

1.4 Problem Definition . . . 3

1.5 Challenges . . . 4

1.6 Proposed Solution . . . 4

1.7 Contributions . . . 5

2 Related Works **6**

2.1 Randomized Input Sampling (RISE) . . . 6

2.2 Local and Surrogate Models . . . 7

2.3 Learning to Perturb . . . 8

3 Methodology **10**

3.1 Problem Definition . . . 10

3.2 Proposed Method: PERT . . . 11

3.3 Prioritized Replacement Selector . . . 12

3.4 Guided Perturbation Function . . . 14

3.5 Optimizing PERT . . . 16

4 Experiments **19**

4.1 Datasets 19

4.2 Compared Methods 20

4.3 Implementation Details 21

4.4 Metrics 21

4.5 Experimental Results 24

4.5.1 PERT successfully finds the most-important timesteps. 24

4.5.2 Ablation Study 26

4.5.3 Hyperparameter Study 29

4.5.4 Case Study 31

5 Conclusion **34**

6 Future Work **35**

6.1 Incorporating distance metrics 35

6.2 Extending to Multi-variate, Multi-class problems 36

6.3 Shared Saliencies 38

List of Figures

1.1 Example of Time Series Saliency Map highlighting input time steps contributing to classification result. 2

2.1 The intuition behind SHAP. The original model f is probed in the vicinity of the specimen, resulting in a linear explanation model g[26] 7

2.2 TSNE visualization of instance perturbations in LIME[32] 9

2.3 TSNE visualization of instance perturbations in MP[9] 9

3.1 PERT Architecture 12

4.1 Deletion and Insertion Metrics 23

4.2 Ablation Study. 26

4.3 PERT Hyperparameter Study 30

4.4 Blip Case Study. 31

4.5 CricketX "No-Ball" Class Case Study 32

6.1 TSNE visualization of instance perturbations in LIME[32] 35

6.2 TSNE visualization of instance perturbations in PERT[9] 35

6.3 Learnable Multi-variate Multi-class Mask 37

List of Tables

4.1 Summary statistics for the real-world datasets and the Accuracy of our corresponding FCN and RNN models. 19

4.2 Performance of the AUC-difference metric with the FCN black-box model. Parentheses indicate σ. Compared methods are separated into four groups: Random perturbation, linear surrogate model, game theory method, and learned perturbations. 25

4.3 Average performance of the AUC-difference metric with the RNN black-box model. 26

4.4 Confidence suppression metric performance for seven key datasets with the FCN black-box model. Lower values are better for Saliency sum and Confidence suppression game, Higher values are better for Saliency variance. $\downarrow$ indicates *the lower the better*. $\uparrow$ indicates *the higher the better*. 27

4.5 Confidence-Suppression Metric performance for two key datasets with the RNN black-box model. Lower values are better for Saliency sum and Confidence suppression game, Higher values are better for saliency variance. 28

Chapter 1

Introduction

1.1 Background

Deep neural networks are the state-of-the-art solution to many time series classification problems across important domains such as healthcare [26, 48] and finance [22, 45]. In such high-risk domains, errors in the predictions by deep neural network models can be catastrophic. However, when developing these deep solutions, it is rarely considered that users rarely trust predictions from "black box" that they do not understand [39].

Meanwhile, model complexity has recently skyrocketed, making these models and their predictions challenging to comprehend. To address this problem, recent works have shown that users are more likely to trust a model's predictions if they are shown *what evidence the model used the most* [9]. Attribution-based explainability methods thus aim to discover to what degree a classifier used each of its input features.

1.2 Motivating Example

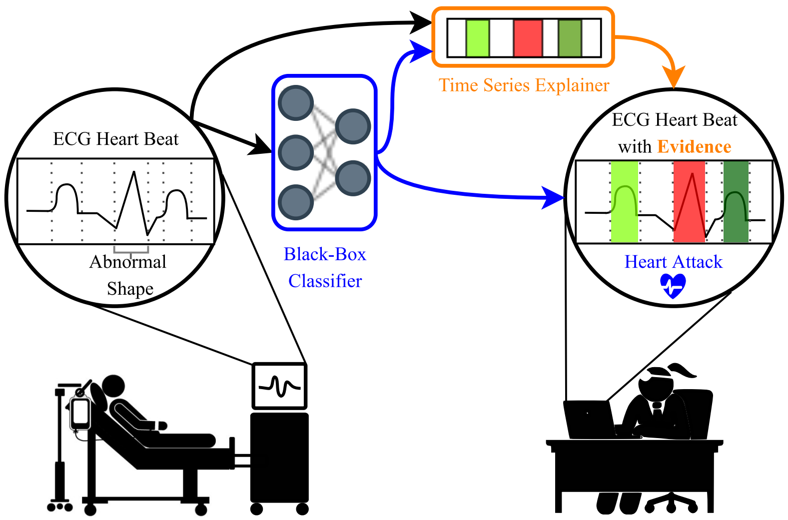

Figure 1.1: Example of Time Series Saliency Map highlighting input time steps contributing to classification result.

Consider a black-box deep time series classifier that detects abnormal heartbeats, or arrhythmia, in ECG data [13, 31]. Without knowing whether or not the model looked at the proper region of the heartbeat, a doctor will not trust its prediction. As shown in Figure 1.1, one solution is to attribute the prediction to the evidence that the model used the most to make its decision. In this example, wave-like shapes are shown in the input ECG time series, one of which is labeled as abnormal. These shapes are all part of a single cardiac cycle. The classifier accurately predicted the ECG is part of a *Heart attack* due to the presence of unexpected spike in the middle of the cycle. Shown in orange, the explainability method finds that the black-box classifier indeed found the unexpected spike as the evidence for this classification, as shown in red. The expected shapes are reported as green bars.

1.3 State-of-the-Art

Recently, attribution-based explainable AI (XAI) has rapidly become popular in the literature [32, 25, 7, 44, 14, 34, 33, 45, 41, 16, 38]. However, most of these XAI methods are designed for images [19, 9, 32, 29, 8, 47, 40, 43] and text [20, 37, 1, 18]. while very little has been done for time series. Time series values are unidirectionally correlated. Also, during classification, short contiguous subsequences often contain much of the discriminative information [46]. However, existing explainability methods treat all input features *independently*, ignoring correlations and possibly disrupting discriminative subsequences.

Some of the most recent and promising explainability methods have begun to derive attribution-based explanations by *perturbing* inputs and then observing the effects on the black-box model's predictions. However, current perturbation strategies are developed specifically for computer vision where images are transformed into the same space (meaning, values ranging from [0 to 255]). By darkening pixels of an image or altering their hues, different qualities of a black-box model can be tested. Unfortunately, these approaches do not have clear analogies for time series where the range of a series' values depends entirely on its domain. Some very recent works [12, 25, 3, 15, 10] have only just begun to fill this gap by adapting image and text approaches for time series.

1.4 Problem Definition

In this work, we study the problem of *Learning Perturbations* to produce attribution-based explanations for a black-box classifier's prediction for a given time series instance. Our goal is to generate a saliency map, or one value per time step of an input time series, where higher values indicate stronger dependence of the model on the time step. A good explanation method must adapt to the specific input instance. This is a multi-objective optimization problem. Namely, a good saliency map must accurately highlight the most relevant time steps while remaining intuitive to the end-user by finding the *fewest* possible time steps.

1.5 Challenges

Despite the importance of explaining deep time series classifiers, three open challenges remain:

- *Heterogeneous series*: Time series within the same dataset can be highly variable, even within the same class. To best explain a classifier's prediction for a given series, a perturbation strategy must be adaptive across both time series and classes.

- *Perturbing long series*: Perturbation methods rely on generating *perturbed* versions of input time series. As the series length increases, the range of possible perturbations grows high. It makes finding perturbations computationally long.

- *Conflicting objectives*: Meaningful explanations are often made at the expense of their accuracy. An explanation highlighting only a few key inputs is intuitive but might fail to explain the model if the black-box actually distributes its focus across many inputs.

1.6 Proposed Solution

To derive attribution-based explanations I propose a model-agnostic, perturbation-based time series explainer - ***PE****rturbation by Prioritized* ***R****eplacemen****T*** (PERT). PERT uses a gradient-based search algorithm to discover the impact of perturbing each time step on the black-box model's predictions, producing a learned saliency map. It jointly learns to sample a replacement time-series from an available background dataset containing many time series using a *prioritized replacement selector*. It regularizes the perturbations to ensure perturbations remain similar to other series the model has seen before. As a result, it this way adapts to the given dataset and better yet to each time step of the instance-of-interest.

1.7 Contributions

Our main contributions are as follows:

- Identify and characterize the open problem of *Learning Perturbations* for deep time series classifiers.

- Propose the first *Learning Perturbations* solution to this open problem which integrates two novel components, jointly learning to solve two tasks: gathering the appropriate time series to aid in perturbation of a specific interest, and *how* to perturb each timestep to best tease out its impact on the model's predictions.

- Using nine popular real-world publicly-available datasets, we conclusively demonstrate that our proposed method performs better on all three proposed metrics compared to five state-of-the-art explainability methods for different types of black-box time series classifiers, for multiple key metrics.

Chapter 2

Related Works

2.1 Randomized Input Sampling (RISE)

In RISE[29], the authors estimate the importance of pixels by dimming the pixels in random combinations and reducing their intensities down to zero. The method uses a binary mask [0,1] to perturb the instance. Using Monte-Carlo sampling, the importance maps are generate empirically by estimating the sum in equation 2.1. A sample set of masks $M_1, ..., M_N$ are used to probe the model by running it on the masked images $I \odot M_i, i = 1, ..., N$. The weighted average of the masks are considered where the weights represents the normalized confidence scores of $f(I \odot M_i)$.

$$S_{I,f}(\lambda) \overset{MC}{\approx} \frac{1}{E[M].N} \sum_{i=1}^{N} f(I \odot M) \cdot M_i(\lambda) \tag{2.1}$$

The approach faces several challenges when operating on time series data. The number of perturbations is directly proportional to the length of the time-series, due to the use of Monte-Carlo sampling and hence does not scale well. The use of binary mask limits the method to work with coarse-grained perturbations which in-turn fails to constrain the search space and the perturbations are created using zero replacement, hence the method is prone to having network artifacts.

2.2 Local and Surrogate Models

To generate a location explanation, the model-agnostic approaches make use of perturbations to understand the learning function in the vicinity of the input to be reasoned. The input is called a specimen and newly generated nearby samples are known as perturbations. For perturbations based on an algorithm, one needs to define a mapping function describing the ways to perturb the specimen. In LIME[32] introduced mappings for images, text, and tabular data. The timeExplain[26] authors develop domain mappings for SHAP[21] specific to its model-agnostic explanation tool - Kernel SHAP.

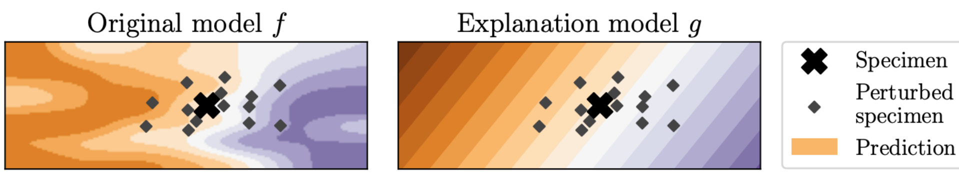

Figure 2.1: The intuition behind SHAP. The original model f is probed in the vicinity of the specimen, resulting in a linear explanation model g[26]

Kernel SHAP the black-box model is a function that maps input space to the classification space, function $f : I \rightarrow R$ disables portions of specimen resulting in perturbed instances and then compute the marginal contributions $f(z)$. On multiple iterations with different perturbation allows the method to explore the behavior of the prediction function f in the vicinity of the specimen. With the newfound knowledge, an interpretable linear model is used to approximate the original model near x. The coefficients for each of the timesteps can be extracted from the interpretable linear models which describe the impact of each time step of x has on the prediction

$f(x)$. However, the approach fails to scale to lengthy time-series instances due to an exponential increase in the number of perturbations required. It simply does not make use of the state of the previous perturbation and the network's response to create a new perturbation.

2.3 Learning to Perturb

Simonyan et.al pioneered saliency maps [39] for visualizing image classification models. The method computes the gradient of the class score concerning the input image. Many approaches have utilized saliency maps to enhance visual explanations. These methods examine the correlation between the inputs and the outputs by perturbing the input instance x and observing the changes in the classifier's sensitivity $f(x)$. They are gradient-based methods, which back-propagates the gradient for a class label to the input layer. Some are not model-agnostic [50, 36, 49] with the exception of [39, 9, 2], many requires network architectural modification [50, 42, 48] and in some cases access to intermediate layers [2, 50, 36, 49].

Meaningful Perturbations The authors of MP[9] has developed a framework to find the part of an image most responsible for a classifier's decision. The image specific method aptly named as deletion game, is model-agnostic and works by deleting regions of input image that are maximally informative in order to explain the behaviour of the blackbox. The goal is to find the smallest deletion mask m that cause the prediction $f(x)$ to drop significantly. The process is formulated as,

$$m^* = \underset{m \in [0,1]}{argmin} \lambda \left\| 1 - m \right\| + f_c(\phi(x; m)) \tag{2.2}$$

where λ incentivizes the objective function to turn of most of the mask i.e, to delete a small subset of the input image x. The deletion game removes enough evidence to prevent the network from recognizing the object in the image. Figures 6.1 and 6.2 showcases the stark contrasts between random perturbations (LIME[32]) and learning to perturb (MP [9]). Each of the figures is the visual representation of perturbations across iterations. LIME perturbs the data 5000 times to derive the explanation whereas MP derives the reason in under 500 perturbations. Each n dimensional perturbated input is mapped to corresponding two-dimensional representation using TSNE[22], a pair-wise distance ranking metric. In MP, the perturbations trace a concise path initially and show variations during the last few iterations denoting the learning capabilities. On the other-hand LIME is agnostic to the progress of iteration indicating the random nature of the perturbations. However, the method uses an image-specific deletion process i.e, replace the deleted part with zeros which do not fare well in the time-series domain. Also, it suffers from explanation bias as a human-centric evaluation metric is used to measure the quality of the explanations.

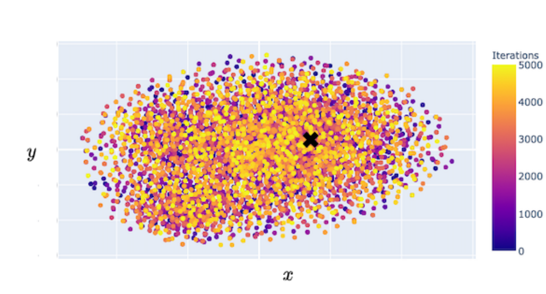

Figure 2.2: TSNE visualization of instance perturbations in LIME[32]

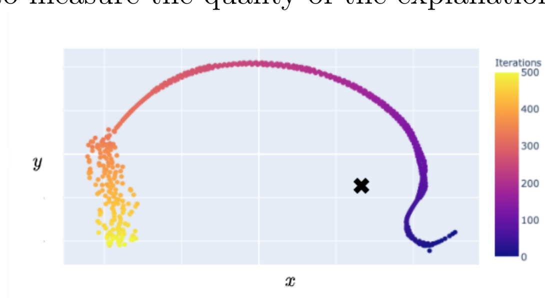

Figure 2.3: TSNE visualization of instance perturbations in MP[9]

Chapter 3

Methodology

3.1 Problem Definition

Assume we are given a set of N time series $\mathcal{D} = \{X^1, \ldots, X^N\}$ and a black-box classifier $f_c : \mathbb{X} \rightarrow \mathcal{Y}$, where $\mathbb{X} \in \mathbb{R}^T$ is the T-dimensional feature space and $\mathcal{Y}$ is the label space. Let us consider one instance-of-interest $X \in \mathcal{D}$ where $X = [x_1, \ldots, x_T]$ along with a class-of-interest C, the prediction for which we would like an explanation.

Our goal is to learn a saliency map $\theta = [\theta_1, \ldots, \theta_T]$ where $\theta_t \in [-1, 1]$ indicates the *importance* of time step t based on their influence on the predicted probability $P(C|X)$ of class C by black-box f_c. The scale of the real-valued θ_t reflects the importance of the corresponding time step x_t.

While the notion of *importance* is challenging to quantify, we follow the lead of recent work on perturbation-based explainability [9, 8] and assume that the aim of saliency is to identify which timesteps of a time series instance X are used by the black box f_c to produce the output value $P(C|X)$. We can do so by observing how the value of $P(C|X)$ changes as X is perturbed. Naturally, the perturbation-based explanation problem is thus to derive a *perturbation function* $f_p(X)$ that can be used to discover the impact of perturbing each time step x_t on the predicted probability of class C. Using this perturbation function, a saliency map θ may be derived. A successfully learned saliency map θ will assign high values to the most-impactful time steps, effectively ranking them by their impact on $P(C|X)$. Intuitively, an explanation that is *simpler* is often easier to understand, and so we also prefer that $\sum_{t=1}^{T} |\theta_t|$ be small so as to encourage unimportant timesteps to go to zero.

3.2 Proposed Method: PERT

To derive an explanation for the class prediction made by a black-box model f_c, we propose a model-agnostic, perturbation-based method specific to time series that uncovers the importance of each timestep to the model's final prediction. We refer to our method as ***PE**rturbation by Prioritized **R**eplacemen**T** (PERT)*. Perturbation involves modifying the time steps from X. As illustrated in Figure 3.1, PERT adaptively employs the dataset $\mathcal{D}$, learning to sample a *replacement* time series R which is used to mix each time step of the instance-of-interest $\hat{X}$ with the corresponding time step from R to create in-distribution perturbations. Furthermore, by querying the black-box model's predictions for a perturbed version of the instance-of-interest X, PERT discovers how sensitive predictions are to perturbations in each times step. To encode these ideas, PERT contains two components: (1) A *Prioritized Replacement Selector* that learns to perform weighted sampling of the time series in $\mathcal{D}$, finding the best replacement time series R specific to instance X and (2) A *Guided Perturbation Function* that learns θ_t to perturb X and discover the impact of each timestep on the black-box model's final prediction. These two steps jointly learn to generate a *saliency map* with the fewest and most impactful timesteps that explain the classifier's prediction.

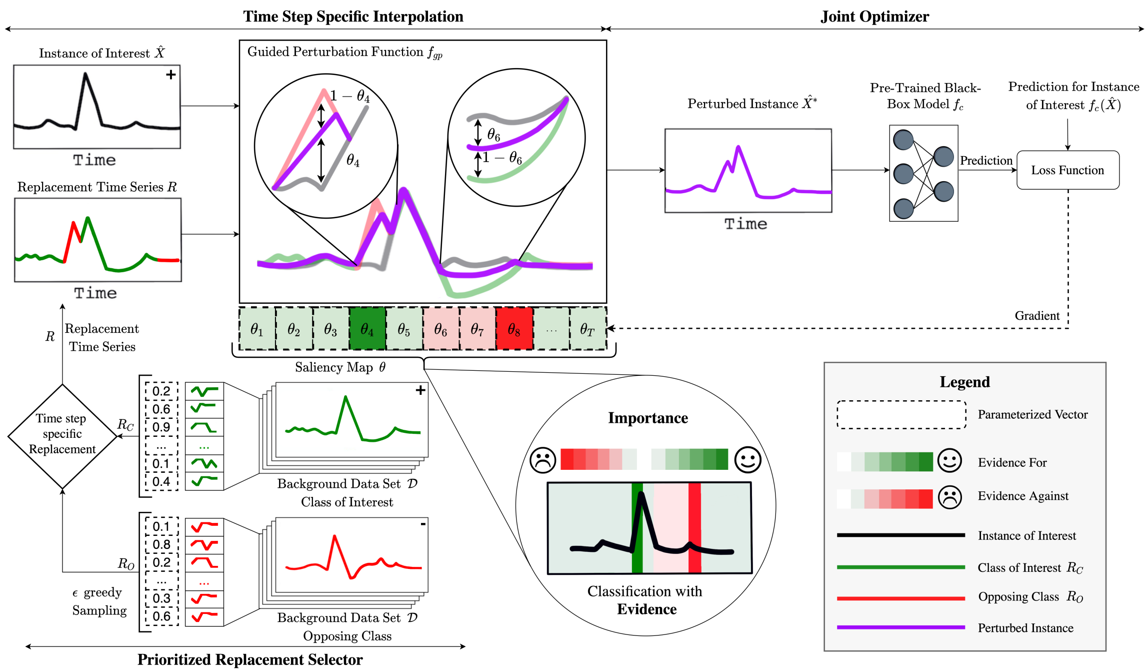

Figure 3.1: PERT Architecture

3.3 Prioritized Replacement Selector

To perturb the values of a time series, we must choose new values to replace them with. However, this choice is highly impactful in time series since the shapes and trends of the signals may be altered dramatically as we show in our Experiments in Section 4.5.2. To avoid such massive changes, which might lead to time series unlike any the classifier has seen before, we instead opt to replace values with those of other time series in dataset $\mathcal{D}$. Thus the task of the first component of PERT, the Prioritized Replacement Selector, is to choose which time series is appropriate to use from the background dataset for replacement of the timesteps of instance X. Intuitively, the choice of best replacement time series may vary by timestep and so we achieve this on a timestep-by-timestep basis, choosing different replacement series and corresponding values for each timestep of X. In practice, to provide evidence both *for* and *against* class C, the Prioritized Replacement Selector chooses two time series representatives R_C and R_O from $\mathcal{D}$ where R_C is a series from class C and R_O is a series not from class C. As discussed in Section 3.4, these series will be used together to generate one final perturbation $\tilde{X}$.

To acquire R_C and R_O, we split $\mathcal{D}$ into two subsets: $\mathcal{D}_C$ contains all samples from the class-of-interest C, and $\mathcal{D}_O = \mathcal{D} - \mathcal{D}_C$ contains all remaining, or opposing, instances. All instances in each set are assigned individual weights w to serve as their *priorities*, similar to Prioritized Experience Replay [35]. We then sample one replacement time series R from each set by using the softmax of the set's respective weights w_O and w_C to parameterize two independent categorical distributions:

$$\mathrm{P}(R_C^i) = w_C^i$$

$$\mathrm{P}(R_O^i) = w_O^i$$

where R_C^i is the i-th instance of dataset $\mathcal{D}_\mathcal{C}$ and w_C^i is its corresponding weight. Intuitively, instances with higher weights w will have a higher likelihood of being selected. Since w will eventually be learned (Section 3.5), the chosen representatives will differ according to the instance X, resulting in adaptive explanations.

As proposed, values of w that are large early in training may be exploited. Therefore, we follow the literature [23] and employ the standard ϵ-greedy approach to balancing *exploration* and *exploitation* while PERT is being trained:

$$R_C = \begin{cases} R_C \text{ (itself)} & \text{with probability } 1 - \epsilon \\ \text{random } R_C \in \mathcal{D}_C & \text{with probability } \epsilon \end{cases} \tag{3.1}$$

Thus when ϵ is large, replacement series are picked randomly and when ϵ is small, weights w are used to select the replacement series. Selection of R_O is performed the same way. To encourage early exploration and later exploitation, ϵ is exponentially decayed during training.

3.4 Guided Perturbation Function

Next, we compute the perturbation $\tilde{X}$, which is a modified version of instance X using our *Guided Perturbation Function* and replacement series R_C and R_O. $\tilde{X}$ will subsequently be fed to the black-box model f_c to observe how this perturbation has affected its prediction. To achieve this, we *learn* a perturbation function $f_{\text{p}} : \mathbb{X} \rightarrow \mathbb{X}$. The key component of f_{p} is a vector of learnable weights $\theta \in [-1, 1]^T$, which will serve as the final saliency map and be the explanation of the model's prediction. Higher values of θ indicate stronger evidence *for* class C while lower values are evidence *against* class C

To take into account both evidence *for* and *against* class C, our perturbation function f_{p} chooses between replacing values at each timestep with those from R_C and R_O adaptively. To make it so that $\theta_t < 0$ indicates that its corresponding time step X_t is evidence *against* class C, we replace the time step with R_C, the representative of class C. Similarly, when $\theta_t \geq 0$, X_t is replaced with the corresponding timestep of R_O. This way, PERT learns the degree of sensitivity of each time step. The function f_{p} generates its final perturbation $\tilde{X}$ by performing *timestep-specific interpolation*:

$$\tilde{X} = \theta \odot X + (1 - \theta) \odot (1_{\theta<0} \odot R_C + 1_{\theta\geq 0} \odot R_O) + g \tag{3.2}$$

where $1_{\theta<0}$ is a vector-wise indicator function that returns 1 for elements of θ that are less than 0 and $1_{\theta\geq 0}$ returns 1 for elements of θ greater than or equal to 0. $\odot$ is the Hadamard product. For readability, we refer to this operation as function $f_{\text{p}}(X; \theta)$. In practice, we also add a small amount of Gaussian noise g to avoid overfitting θ to extremely specific values, similar to [9]. Using Equation 3.4, the final values of $\tilde{X}$ are thus interpolations between the original timesteps of X and the replacement series R_C or R_O according to the scale of the corresponding value in θ.

Once perturbation $\hat{X}^*$ is obtained, we can compare the original prediction, the black-box model f_c's prediction on $\hat{X}$, to $P(C|\hat{X}^*)$, the prediction given the perturbation as input. The intuition behind adaptive time step specific interpolation is given by the three possible relationships between $P(C|\hat{X}^*)$ and $P(C|\hat{X})$,

- $\boldsymbol{P(C|\hat{X}^*) < P(C|\hat{X})}$. By perturbing $\hat{X}$, the model's confidence in class C decreases. We intentionally insert authentic opposing information, different from that of $\hat{X}$ avoiding the creation of out-of-distribution perturbations (i.e, replace the value of t with the corresponding value of time step from an instance of opposing class $R_{O(t)}$). If the original values of t were crucial to the prediction $P(C|\hat{X})$, replacing it with $R_{O(t)}$ must result in a drop in $P(C|\hat{X})$.

- $\boldsymbol{P(C|\hat{X}^*) = P(C|\hat{X})}$. Perturbing $\hat{X}$ has no impact on $P(C|\hat{X})$, indicating independence between the input features and the output prediction according to f_c. Finding these two predictions to be exactly equal is expected to be exceedingly rare, depending on computation precision, but as these two quantities approach one another, the intuition holds.

- $\boldsymbol{P(C|\hat{X}^*) > P(C|\hat{X})}$. Perturbing $\hat{X}$ causes the predicted likelihood of class C to increase. This indicates that the original values of $\hat{X}$ are *negatively* correlated to the prediction of class C. We purposefully replace the value of t with the corresponding value of sampled timeseries instance from the same class $R_{C(t)}$. This is done to ensure that the $P(C|\hat{X})$ is preserved in order to derive a local explanation for $\hat{X}$, as inserting authentic opposing information leads to an increase in $P(C|\hat{X})$, thereby failing to explain $\hat{X}$ for the given $P(C|\hat{X})$.

We initialize the values of θ uniformly between $-1e^{-2}$ and $1e^{-2}$ to encode no prior assumptions on which time steps are most important and are iteratively updated throughout the training. We start with small values for θ and thus perform *forward selection*, steadily inserting only the most crucial timesteps to the prediction $P(C|\hat{X})$. This way, we encourage the system to provide simpler explanations, as the default sum of θ is small. Alternatively, θ can be initialized to be close to 1 and followed by *backward* selection. However, we show in our experiments 4.2 that this approach is inferior.

3.5 Optimizing PERT

A major benefit of *learning to perturb* for explainability is that many behaviors of good explanations can be encouraged during optimization via a loss function. In this work, we learn the saliency values θ iteratively with respect to a novel loss function (Equation 3.6) that contains three key components, each of which works together to provide accurate and simple explanations for a black-box time series classifier. There are three components in our loss function: $L_{\text{preservation}}$, L_{budget} , and L_{TV}. The first component, $L_{\text{preservation}}$ encourages the perturbation function f_p to produce perturbations for which the black-box classifier makes the *same* prediction as it did for the instance-of-interest $\hat{X}$:

$$L_{\text{preservation}} = \lambda_1 \left(\frac{1}{\left\|\hat{X}\right\|} \sum_{t=0}^{T} (f_c(\hat{X}) - f_c(f_p(\hat{X};\theta)))^2 \right) \tag{3.3}$$

where $f_c(\hat{X})$ is black-box classifier's predicted probability for the instance-of-interest $\hat{X}$ and $f_c(\hat{X}^*)$ is black-box classifier's prediction for the perturbed instance X^*. By minimizing the squared difference between these terms, we encourage f_p

to *preserve* the prediction made on $\hat{X}$. To balance the goal of explainability and simplicity, we incorporate a L_{budget} on the saliency values, it encourages the final saliency values θ to be small with fewest possible timesteps:

$$L_{\text{budget}} = \lambda_2 \left(\frac{1}{\|\theta\|} \sum_{t=0}^{T} |\theta_t| \right) \tag{3.4}$$

Third, we add the intuition that neighboring timesteps and short contiguous subsequences should be roughly equal in importance. We achieve this through *Total Variance Normalization* [9], minimizing the squared difference between neighboring saliency values:

$$L_{\text{TV}} = \lambda_3 \left(\frac{1}{\|\theta\|} \sum_{t=0}^{T-1} (\theta_t - \theta_{t+1})^2 \right) \tag{3.5}$$

Finally, the loss terms are summed and each is associated with a coefficient to allow for re-scaling depending on task-specific preferences in explanation behavior. We scale the final loss function according to the sampling weights w_O and w_C.

The final loss for PERT is shown in Equation 3.6.

$$L(P(\hat{X});\theta) = (L_{\text{preservation}} + L_{\text{budget}} + L_{\text{TV}}) * \frac{1}{2}(w_O + w_C) \tag{3.6}$$

We jointly optimize θ and w by minimizing $L(P(\hat{X});\theta)$. To prioritize the replacement time series R_C and R_O which help minimize $L(P(\hat{X});\theta)$, we use $L(P(\hat{X});\theta)^{-1}$ to update the corresponding replacement sample weights w_O and w_C.

Algorithm 1 PERT

Input: $\hat{X}$, f_c, $\mathcal{D}$

Result: Saliency map $\hat{S}$

$\theta \leftarrow random\_uniform(low = -1e - 2, high = 1e - 2)$

for *epoch in range(epochs);* **do**

$R_O, R_C, w_O, w_C \leftarrow$ Prioritized Replacement Selector$(\hat{X}, \mathcal{D})$

$X^* \leftarrow \theta \odot X + (1 - \theta) \odot (1_{\theta<0} \odot R_C + 1_{\theta\geq 0} \odot R_O) + g_n$

$L_{\text{preservation}} \leftarrow \lambda_1 \left(\frac{1}{\|\hat{X}\|} \sum_{t=0}^{T} (f_c(\hat{X}) - f_c(X^*))^2 \right)$

$L_{\text{budget}} \leftarrow \lambda_2 \left(\frac{1}{\|\theta\|} \sum_{t=0}^{T} |\theta_t| \right)$

$L_{\text{TV}} \leftarrow \lambda_3 \left(\frac{1}{\|\theta\|} \sum_{t=0}^{T-1} (\theta_t - \theta_{t+1})^2 \right)$

$L(P(\hat{X}); \theta) \leftarrow (L_{\text{preservation}} + L_{\text{budget}} + L_{\text{TV}}) * \frac{1}{2}(w_O + w_C)$

$\theta \leftarrow \theta - \eta \nabla J(\theta)$

update_priorities$(L(P(\hat{X}); \theta)^{-1})$

clamp$(\theta, low = -1, high = 1)$

end

Chapter 4

Experiments

4.1 Datasets

We evaluate our method on nine real-world time-series datasets: WAFER [27], GUNPOINT [30], COMPUTERS [6], EARTHQUAKES [6], FORDA [6], FORDB [6], CRICKETX [6], PTB [11], ECG [27].

Each is a popular and publicly-available dataset for time series classification, and the summary statistics are provided in Table 4.1. For each dataset, we train a three-layered Fully-Connected Network (FCN) and a multi-node Recurrent Neural Network (RNN) to serve as black-box classifiers in need of explanations. Both models achieve nearly state-of-the-art performance for each task. Each dataset comes with default train and test splits.

Dataset	WAFER	GUNPOINT	COMPUTERS	EARTHQUAKES	FORDA	FORDB	CRICKETX	PTB	ECG
Num. Train Instances	1000	50	250	322	3601	3636	390	1456	100
Num. Test Instances	6164	150	250	139	1320	810	390	1456	100
Num. Timesteps	152	150	720	512	500	500	300	187	96
FCN Accuracy (%)	99	99	80	75	96	92	81	98	98
RNN Accuracy (%)	99	99	79	75	96	92	80	98	98

Table 4.1: Summary statistics for the real-world datasets and the Accuracy of our corresponding FCN and RNN models.

4.2 Compared Methods

We compare our proposed method, PERT, to one baseline and five state-of-the-art explanation methods for both FCN and RNN black-box models.

- ***Random***. Each time step is assigned a random saliency value between -1 to 1 from a uniform distribution. This approach serves as a baseline for all methods.
- ***RISE*** [29]. The partial derivative of the black-box model's prediction $P(C|\hat{X})$ with respect to each time step is estimated empirically by randomly setting timesteps to zero and summarizing its impact on the $P(C|\hat{X})$.
- ***LEFTIST*** [12]. The partial derivative of $P(C|\hat{X})$ with respect to each time step is estimated empirically by randomly *replacing* the timestep with a corresponding value from a random instance from the background dataset and summarizing its impact on $P(C|\hat{X})$.
- ***LIME*** [32]. Saliency values are derived from the coefficients of a linear surrogate model, trained to mimic the behavior of the black-box model in the feature space surrounding $\hat{X}$. The success of this approach relies on the model behaving linear locally, which is rarely guaranteed in practice.
- ***SHAP*** [19]. SHAP assigns Shapley values [5] to each time step, thus computing their contributions to $P(C|\hat{X})$. Each time step is replaced by every value observed at the corresponding time step across all other instances in the background dataset.
- ***Meaningful Perturbation (MP)*** [9]. MP learns to perturb each time step such that $P(C|\hat{X})$ decreases. Perturbation is achieved by combining squared

exponential smoothing with additive gaussian noise. Saliency values are then learned iteratively and are ultimately used as the final explanation.

4.3 Implementation Details

For each dataset, we train a three-layer FCN and a 10-node single layer RNN with GRU cells to serve as black-box time series classifiers in need of explanations. We train each model only on the training data, then explain their predictions for all testing instances using each compared explainability method. All reported metrics are the result of averaging over five runs to estimate the variance of the explainability methods.

We optimize our proposed method using Adam [17] with a learning rate of $1e^{-3}$ and train for 5000 epochs, which empirically achieves convergence. We used Weights & Biases [4] for experiment tracking and visualization. Our proposed method is implemented in PyTorch [28] and our code is publicly-available at `https://github.com/kingspp/timeseries-explain`

4.4 Metrics

Careful selection of evaluation metrics plays a crucial role in our research. It is extremely difficult to judge the quality of the explanation due to the absence of *standardized models* and the *unintuitive* nature of time-series data. It is an arduous task to debug and conclude whether the error is due to the proposed solution, the chosen model, or the classifier design. The presence of multiple dynamic probabilistic components makes it a challenge to evaluate the quality of the solution from the perspective of model interpretation. We plan to use causal metrics for evaluation. Explanation methods evaluated in a human-centered way, where there exists "ground truth" regions or bounding boxes drawn by humans and the generated saliency maps are compared against, are laborious and biased. The deeplearning models are capable of constructing meaningful representations that are non-intuitive to humans. Thus, having human-out-of-the-loop metric for evaluation makes it fair and true to the classifier's view on the problem.

We use three key metrics to evaluate saliency maps for time series under the intuition that a prediction is well-explained if it accurately ranks the timesteps by their importance, as defined by changes in $P(C|\hat{X})$ *and* returns only the most-important timesteps.

AUC Difference. Saliency maps can be evaluated by "inserting" or "deleting" timesteps from the time-series instance based on the derived importance map and observing the changes in the black-box model's predictions [29].

Intuitively, a good saliency map is one that has ranked timesteps such that when the most important timesteps are deleted, there is a sharp drop in the confidence of the model's prediction. This can be measured by computing the area under the *deletion* curve (AUDC) as timesteps are deleted one by one. A lower value for this area naturally indicates a better explanation. Analogously, insertion of a few important timesteps should result in the largest possible increase in the confidence of the model's prediction, thereby creating a large area under the *insertion* curve (AUIC). To ease comparisons, we merge these two measures into one metric by computing the difference, AUC-Difference = AUIC − AUDC. Ideally, the difference should be large (1.0), implying the saliency maps having a high AUIC (1.0) and a low AUDC (0.0) is a good explanation. This metric alleviates the need for human evaluation and annotation and makes it more fair and true to the classifier's own view on the problem. To achieve deletion during evaluation we replace a to-be-deleted timestep with the corresponding timestep from the opposing class's mean. Conversely, for insertion, we iteratively replace the mean time series from the opposing class with the original inputs of the instance-of-interest. Figure 4.1 describes the ideal case of an explanation with an AUIC score of 0.84 and AUDC score of 0.05 resulting in AUDC score of 0.79.

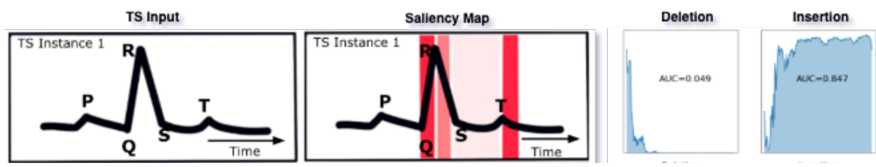

Figure 4.1: Deletion and Insertion Metrics

Confidence Suppression Game. Another popular approach to evaluating saliency maps is to find the smallest number of timesteps required to suppress the confidence of the black-box model by a given percentage [9]. We thus ask each explanation to play this *Confidence Suppression Game* and return the proportion of timesteps that must be deleted to reduce $P(C|\hat{X})$ by each value in a set of percentages. To achieve deletion, we once again replace timesteps with corresponding values from the opposing class mean.

Minimality of Saliency Maps. A good explanation returns *only* the most important timesteps, thus allowing a user to consider only a few regions of the input. Thus we compute the *sum* of a saliency map, under the intuition that it should be small, as the goals of explainability and simplicity are jointly optimized, we expect importance of unimportant timesteps to go to zero leading to simpler explanations with fewest possible timesteps. To avoid naive solutions with very small and equally distributed saliency values, we report the normalized *variance* of the saliency map. A high variance indicates a larger difference between the minimum and maximum saliency values.

4.5 Experimental Results

4.5.1 PERT successfully finds the most-important timesteps.

First, we measure how well all compared explainability methods have *ranked* the timesteps by their importance via the AUC-Difference metric discussed in Section 4.4. Our results using Fully-Connected Network and Recurrent Neural Network can be found in Tables 4.2 and 4.3 respectively. In all cases, PERT significantly outperforms all other methods, with the largest improvement seen in the Wafer, Gun-Point, Computers, FordA, FordB, and CricketX datasets. This strongly indicates that the saliency maps produced by PERT have indeed ranked the timesteps far more accurately in terms of their individual effect on the black-box model's prediction confidence $P(C|\hat{X})$. We also note that in general, learning to perturb (PERT and MP) outperforms the random-replacement methods (Random, RISE, LEFTIST), linear surrogate method (LIME) and game theory method (SHAP), demonstrating the value in this class of perturbation-based explainability methods. When time series instances are short, such as for the GunPoint and Wafer datasets, RISE and SHAP produce comparable results to PERT as they rely on a densely-sampled feature space surrounding each instance-of-interest. For longer series, covering this space efficiently becomes extremely challenging, motivating *learned* perturbation [9]. We can see a similar pattern in results with FCN and RNN networks on the same datasets.

Next, we use the *Confidence Suppression Game* to measure the smallest number of timesteps that must be deleted to have the black-box model's prediction drop by a set of percentages. We report our findings for the Wafer, ECG, Computers, Earthquakes, Ford-A, Ford-B, and CriketX datasets in Table 4.4, and due to the space constraints the remainder of the results for PTB and GunPoint datasets are included with our publicly-available code, where we find the same trends. Overall, PERT successfully achieves the desired suppression levels by deleting far fewer timesteps than the compared methods. This indicates that PERT indeed finds the fewest and most important timesteps. As expected, all methods also outperform the *Random* baseline with very few exceptions. We also find the same trend to be true for the RNN classifier, the results for which are included with our publicly-available code.

Finally, we use *Minimality of Saliency* as a measure of simplicity of the derived saliency map. The results in Table 4.4 indicates that the saliency maps derived by PERT indeed highlight the fewest possible timesteps necessary to maintain f_c's prediction of $P(C|\hat{X})$ compared to state-of-the-art methods. The high variance of saliency maps demonstrates PERT's ability to avoid naive solutions with small saliency values.

Methods	**Datasets**								
	Wafer	GunPoint	Computers	Earthquakes	FordA	FordB	CricketX	PTB	ECG
Random	-0.02 (.01)	0.02 (.01)	0.01 (.01)	-0.01 (.01)	-0.03 (.01)	-0.01(.01)	-0.01 (.01)	0.06 (.04)	0.01 (.06)
RISE [29]	0.22 (.01)	0.16 (.01)	-0.01 (.02)	0.23 (.05)	0.15 (.02)	0.11 (.01)	0.42 (.01)	0.07 (.05)	0.14 (.07)
LEFTIST [12]	0.53 (.02)	0.15 (.03)	-0.16 (.01)	0.15 (.03)	0.16 (.01)	0.15 (.01)	-0.01 (.01)	0.51 (.01)	0.55 (.01)
LIME [32]	0.06 (.01)	0.10 (.01)	0.06 (.03)	-0.01 (.01)	0.01 (.02)	0.01 (.01)	-0.01 (.01)	0.18 (.07)	0.09 (.06)
SHAP [19]	-0.19 (.01)	-0.01 (.01)	0.10 (.01)	0.71 (.03)	0.23 (.01)	-0.17 (.01)	0.09 (.01)	-0.15 (.01)	-0.11 (.09)
MP [9]	0.49 (.01)	0.03 (.01)	0.15 (.01)	0.33 (.01)	0.48 (.01)	0.37 (.01)	0.43 (.01)	0.33 (.01)	-0.16 (.00)
PERT	**0.74 (.01)**	**0.56 (.01)**	**0.95 (.01)**	**0.93 (.01)**	**0.83 (.01)**	**0.82 (.01)**	**0.69 (.01)**	**0.58 (.01)**	**0.60 (.01)**

Table 4.2: Performance of the AUC-difference metric with the FCN black-box model. Parentheses indicate σ. Compared methods are separated into four groups: Random perturbation, linear surrogate model, game theory method, and learned perturbations.

Methods	Datasets								
	Wafer	GunPoint	Computers	Earthquakes	FordA	FordB	CricketX	PTB	ECG
Random	0.01 (.01)	0.03 (.01)	0.01 (.01)	0.04 (.01)	0.01 (.01)	0.01(.01)	-0.01 (.01)	0.07 (.04)	0.01 (.06)
RISE [29]	0.13 (.01)	0.10 (.01)	-0.01 (.02)	0.23 (.05)	0.15 (.01)	0.11 (.02)	0.42 (.01)	0.10 (.05)	0.19 (.07)
LEFTIST [12]	0.16 (.01)	0.15 (.03)	-0.16 (.01)	0.53 (.03)	0.15 (.02)	0.15 (.01)	-0.10 (.01)	0.42 (.01)	0.51 (.01)
LIME [32]	0.07 (.01)	0.02 (.01)	0.05 (.03)	-0.02 (.01)	0.01 (.01)	0.01 (.01)	0.03 (.01)	0.12 (.07)	0.09 (.06)
SHAP [19]	-0.15 (.01)	-0.01 (.01)	0.10 (.01)	**0.80 (.03)**	0.23 (.01)	-0.17 (.01)	0.30 (.01)	-0.14 (.01)	0.08 (.09)
MP [9]	0.55 (.01)	0.02 (.01)	0.16 (.01)	0.30 (.01)	0.47 (.01)	0.39 (.01)	0.23 (.01)	0.30 (.01)	-0.15 (.01)
PERT	**0.78 (.01)**	**0.48 (.01)**	**0.92 (.01)**	**0.82 (.01)**	**0.70 (.01)**	**0.70 (.01)**	**0.68 (.01)**	**0.52 (.01)**	**0.57 (.01)**

Table 4.3: Average performance of the AUC-difference metric with the RNN black-box model.

4.5.2 Ablation Study

We next compare alternative approaches to some of PERT's key components with respect to the AUC-Difference metric, the results for which are shown in Figure 4.2. We target this study at three categories: loss components, selection criteria, and replacement strategies. First, we compare PERT's performance while removing different components of the loss function. As expected, $L_{\text{preservation}}$ clearly has the largest impact on the final AUC-Difference, as without this component, there is no relationship between the saliency map and the model's prediction. The remaining components g_n, L_{Budget} and L_{TVNorm} have less of an impact but still contribute to PERT's state-of-the-art performance.

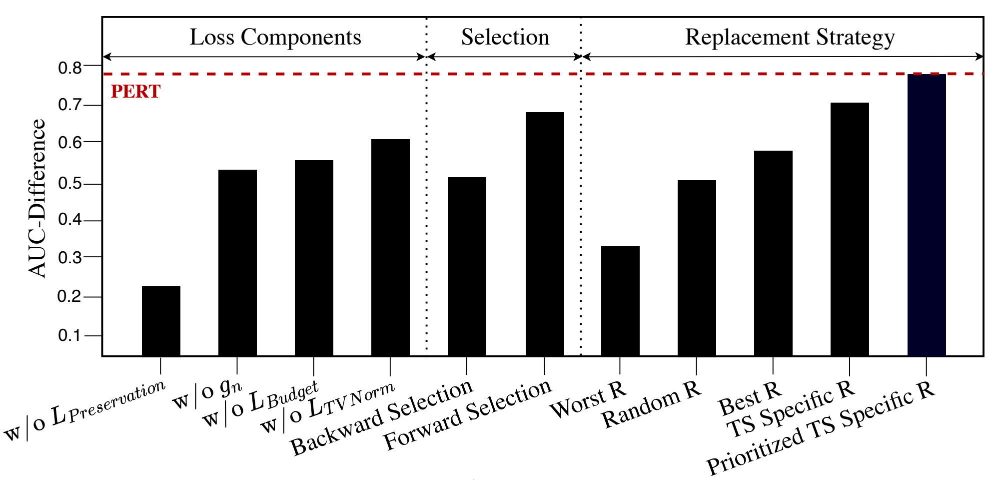

Figure 4.2: Ablation Study.

Second, PERT uses *Forward Selection*, starting with small saliency values and

		Confidence suppression game ↓										Minimality of Saliency	
Dataset	Method	10%	20%	30%	40%	50%	60%	70%	80%	90%	95%	Sum (%) ↓	$\|Variance\|$ ↑
	Random	0.79	0.82	0.86	0.87	0.87	0.88	0.89	0.91	0.91	0.92	50	0.0016
	RISE [29]	0.57	0.57	0.58	0.59	0.59	0.59	0.61	0.61	0.61	0.61	82	0.0001
	LEFTIST [12]	0.56	0.57	0.58	0.58	0.58	0.58	0.58	0.58	0.58	0.59	78	0.0001
WAFER [27]	LIME [32]	0.69	0.73	0.82	0.82	0.83	0.84	0.84	0.86	0.86	0.88	42	0.0001
	SHAP [19]	0.78	0.78	0.78	0.78	0.78	0.78	0.79	0.79	0.79	0.79	52	0.0004
	MP [9]	0.41	0.47	0.53	0.54	0.55	0.56	0.57	0.58	0.68	0.73	6	0.0041
	PERT	**0.40**	**0.40**	**0.46**	**0.47**	**0.48**	**0.49**	**0.51**	**0.53**	**0.55**	**0.59**	**1**	**0.0153**
	Random	0.40	0.41	0.41	0.43	0.43	0.43	0.44	0.45	0.45	0.45	50	0.0001
	RISE [29]	0.40	0.40	0.40	0.40	0.40	0.41	0.41	0.41	0.41	0.41	76	0.0001
ECG [6]	LEFTIST [12]	0.30	0.30	0.30	0.30	0.30	0.31	0.31	0.31	0.31	0.31	60	0.0001
	LIME [32]	0.71	0.72	0.74	0.77	0.79	0.81	0.81	0.84	0.85	0.64	42	0.0001
	SHAP [19]	0.62	0.62	0.62	0.63	0.63	0.63	0.63	0.64	0.64	0.64	64	0.0001
	MP [9]	0.51	0.51	0.51	0.52	0.52	0.52	0.52	0.52	0.53	0.53	3	0.0005
	PERT	**0.21**	**0.21**	**0.21**	**0.21**	**0.21**	**0.22**	**0.22**	**0.22**	**0.22**	**0.22**	**2**	**0.0034**
	Random	0.69	0.73	0.75	0.77	0.79	0.81	0.83	0.85	0.90	0.95	50	0.0001
	RISE [29]	0.92	0.92	0.93	0.93	0.93	0.94	0.94	0.94	0.94	0.94	46	0.0001
Computers [6]	LEFTIST [12]	1.00	1.00	1.00	1.00	1.00	1.00	1.00	1.00	1.00	1.00	49	0.0001
	LIME [32]	0.60	0.62	0.65	0.68	0.7	0.71	0.73	0.75	0.78	0.82	23	0.0001
	SHAP [19]	0.99	0.99	0.99	0.99	0.99	1.00	1.00	1.00	1.00	1.00	51	0.0001
	MP [9]	0.75	0.76	0.78	0.81	0.81	0.82	0.82	0.83	0.84	0.88	4	0.0005
	PERT	**0.50**	**0.50**	**0.50**	**0.51**	**0.51**	**0.51**	**0.51**	**0.51**	**0.51**	**0.51**	**2**	**0.0017**
	Random	0.97	0.97	0.98	0.98	0.99	0.99	0.99	0.99	1.00	1.00	50	0.0001
	RISE [29]	0.99	0.99	0.99	0.99	0.99	0.99	0.99	0.99	0.99	0.99	74	0.0001
Earthquakes [6]	LEFTIST [12]	0.99	0.99	0.99	0.99	0.99	0.99	0.99	0.99	1.00	1.00	61	0.0001
	LIME [32]	0.98	0.98	0.98	0.98	0.98	0.98	0.98	0.98	0.99	0.99	43	0.0001
	SHAP [19]	0.99	0.99	0.99	0.99	1.00	1.00	1.00	1.00	1.00	1.00	51	0.0001
	MP [9]	0.96	0.96	0.96	0.96	0.96	0.96	0.96	0.96	0.96	0.96	4	0.0001
	PERT	**0.96**	**0.96**	**0.96**	**0.96**	**0.96**	**0.96**	**0.96**	**0.96**	**0.96**	**0.96**	**2**	**0.0039**
	Random	0.75	0.78	0.82	0.84	0.86	0.88	0.89	0.91	0.92	0.95	50	0.0001
	RISE [29]	0.76	0.76	0.76	0.76	0.76	0.76	0.77	0.77	0.77	0.78	55	0.0001
Ford-A [6]	LEFTIST [12]	0.78	0.78	0.79	0.80	0.81	0.82	0.83	0.84	0.84	0.85	49	0.0001
	LIME [32]	0.71	0.75	0.78	0.81	0.83	0.84	0.86	0.87	0.89	0.92	44	0.0001
	SHAP [19]	0.93	0.98	0.98	0.98	0.99	0.99	0.99	0.99	0.99	0.99	47	0.0001
	MP [9]	0.66	0.67	0.70	0.72	0.75	0.77	0.78	0.81	0.83	0.87	3	0.0010
	PERT	**0.63**	**0.64**	**0.65**	**0.66**	**0.66**	**0.67**	**0.67**	**0.68**	**0.69**	**0.72**	**2**	**0.0012**
	Random	0.73	0.74	0.77	0.79	0.81	0.83	0.84	0.85	0.86	0.88	50	0.0001
	RISE [29]	0.73	0.81	0.85	0.86	0.86	0.86	0.86	0.86	0.87	0.87	48	0.0001
Ford-B [6]	LEFTIST [12]	0.72	0.73	0.75	0.77	0.80	0.82	0.83	0.84	0.85	0.86	49	0.0001
	LIME [32]	0.71	0.72	0.74	0.77	0.79	0.81	0.81	0.84	0.85	0.87	30	0.0001
	SHAP [19]	0.71	0.72	0.74	0.75	0.77	0.81	0.81	0.82	0.83	0.84	40	0.0009
	MP [9]	0.71	0.71	0.73	0.74	0.76	0.77	0.78	0.79	0.82	0.83	4	0.0008
	PERT	**0.70**	**0.71**	**0.71**	**0.72**	**0.73**	**0.73**	**0.74**	**0.74**	**0.76**	**0.77**	**2**	**0.0010**
	Random	0.21	0.27	0.35	0.41	0.49	0.61	0.72	0.89	0.93	1.00	50	0.0001
	RISE [29]	0.15	0.15	0.26	0.35	0.45	0.55	0.63	0.91	0.91	0.95	74	0.0001
CricketX [24]	LEFTIST [12]	0.20	0.26	0.29	0.29	0.30	0.50	0.50	0.50	0.50	0.50	51	0.0001
	LIME [32]	0.14	0.19	0.23	0.26	0.29	0.31	0.34	0.37	0.41	0.48	39	0.0001
	SHAP [19]	0.19	0.29	0.33	0.36	0.38	0.39	0.40	0.41	0.43	0.45	33	0.0005
	MP [9]	0.09	0.11	0.12	0.15	0.17	0.18	0.19	0.21	0.21	0.25	2	**0.0040**
	PERT	**0.06**	**0.07**	**0.07**	**0.08**	**0.08**	**0.09**	**0.10**	**0.11**	**0.12**	**0.15**	**1**	**0.0037**

Table 4.4: Confidence suppression metric performance for seven key datasets with the FCN black-box model. Lower values are better for Saliency sum and Confidence suppression game, Higher values are better for Saliency variance. ↓ indicates *the lower the better*. ↑ indicates *the higher the better*.

		Confidence suppression game ↓										**Minimality of Saliency**	
Dataset	Method	10%	20%	30%	40%	50%	60%	70%	80%	90%	95%	Sum (%) ↓	$\|Variance\|$ ↑
	Random	0.75	0.78	0.82	0.83	0.83	0.84	0.85	0.87	0.87	0.88	50	0.0001
	RISE [29]	0.63	0.63	0.64	0.65	0.65	0.65	0.67	0.67	0.67	0.67	82	0.0001
	LEFTIST [12]	0.83	0.84	0.85	0.85	0.85	0.85	0.85	0.85	0.85	0.86	76	0.0001
WAFER [27]	LIME [32]	0.62	0.66	0.75	0.75	0.76	0.77	0.77	0.79	0.79	0.81	44	0.0001
	SHAP [19]	0.74	0.74	0.74	0.74	0.74	0.74	0.75	0.75	0.75	0.75	51	0.0004
	MP [9]	0.41	0.47	0.53	0.54	0.55	0.56	0.57	0.58	0.68	0.73	6	0.0041
	PERT	**0.37**	**0.40**	**0.43**	**0.44**	**0.45**	**0.46**	**0.48**	**0.52**	**0.52**	**0.56**	**3**	**0.0062**
	Random	0.40	0.41	0.41	0.43	0.43	0.43	0.44	0.45	0.45	0.45	50	0.0001
	RISE [29]	0.49	0.49	0.49	0.49	0.49	0.50	0.50	0.50	0.50	0.50	69	0.0001
ECG [6]	LEFTIST [12]	0.65	0.65	0.65	0.65	0.65	0.66	0.66	0.66	0.66	0.66	62	0.0001
	LIME [32]	0.71	0.72	0.74	0.77	0.79	0.81	0.81	0.84	0.85	0.64	40	0.0001
	SHAP [19]	0.64	0.65	0.67	0.70	0.72	0.74	0.74	0.77	0.78	0.57	61	0.0001
	MP [9]	0.45	0.45	0.45	0.46	0.46	0.46	0.46	0.46	0.47	0.47	4	0.0005
	PERT	**0.15**	**0.15**	**0.15**	**0.15**	**0.15**	**0.16**	**0.16**	**0.16**	**0.16**	**0.16**	**2**	**0.0033**
	Random	0.67	0.71	0.73	0.75	0.77	0.79	0.81	0.83	0.88	0.93	50	0.0001
	RISE [29]	0.73	0.73	0.74	0.74	0.74	0.75	0.75	0.75	0.75	0.75	48	0.0001
Computers [6]	LEFTIST [12]	1.00	1.00	1.00	1.00	1.00	1.00	1.00	1.00	1.00	1.00	45	0.0001
	LIME [32]	0.55	0.57	0.60	0.63	0.65	0.66	0.68	0.70	0.73	0.77	24	0.0001
	SHAP [19]	0.99	0.99	0.99	0.99	0.99	1.00	1.00	1.00	1.00	1.00	51	0.0001
	MP [9]	0.60	0.61	0.63	0.66	0.66	0.67	0.67	0.68	0.69	0.73	6	0.0005
	PERT	**0.13**	**0.16**	**0.16**	**0.17**	**0.17**	**0.17**	**0.17**	**0.17**	**0.17**	**0.17**	**3**	**0.0013**
	Random	0.99	0.99	1.00	1.00	1.00	1.00	1.00	1.00	1.00	1.00	50	0.0001
	RISE [29]	1.00	1.00	1.00	1.00	1.00	1.00	1.00	1.00	1.00	1.00	79	0.0001
Earthquakes [6]	LEFTIST [12]	0.96	0.96	0.96	0.96	0.96	0.96	0.96	0.96	0.97	0.97	61	0.0001
	LIME [32]	0.92	0.92	0.92	0.92	0.92	0.92	0.92	0.92	0.93	0.93	45	0.0001
	SHAP [19]	1.00	1.00	1.00	1.00	1.00	1.00	1.00	1.00	1.00	1.00	50	0.0001
	MP [9]	0.83	0.83	0.83	0.83	0.83	0.84	0.87	0.87	0.87	0.89	4	0.0001
	PERT	**0.77**	**0.77**	**0.77**	**0.77**	**0.77**	**0.77**	**0.77**	**0.77**	**0.77**	**0.77**	**2**	**0.0033**
	Random	0.77	0.80	0.84	0.86	0.88	0.9	0.91	0.93	0.94	0.97	50	0.0001
	RISE [29]	0.75	0.75	0.75	0.75	0.75	0.75	0.76	0.76	0.76	0.77	53	0.0001
Ford-A [6]	LEFTIST [12]	0.58	0.58	0.59	0.60	0.61	0.62	0.63	0.64	0.64	0.65	49	0.0001
	LIME [32]	0.62	0.66	0.69	0.72	0.74	0.75	0.77	0.78	0.80	0.83	41	0.0001
	SHAP [19]	0.90	0.95	0.95	0.95	0.96	0.96	0.96	0.96	0.96	0.96	50	0.0001
	MP [9]	0.68	0.69	0.72	0.74	0.77	0.79	0.80	0.83	0.85	0.89	4	0.0018
	PERT	**0.43**	**0.44**	**0.45**	**0.46**	**0.46**	**0.47**	**0.47**	**0.48**	**0.49**	**0.52**	**3**	**0.0024**
	Random	0.73	0.74	0.77	0.79	0.81	0.83	0.84	0.85	0.86	0.88	50	0.0001
	RISE [29]	0.69	0.77	0.81	0.82	0.82	0.82	0.82	0.82	0.83	0.83	49	0.0001
Ford-B [6]	LEFTIST [12]	0.69	0.70	0.72	0.74	0.77	0.79	0.80	0.81	0.82	0.83	49	0.0001
	LIME [32]	0.66	0.67	0.69	0.72	0.74	0.76	0.76	0.79	0.80	0.82	33	0.0001
	SHAP [19]	0.54	0.55	0.57	0.58	0.60	0.64	0.64	0.65	0.66	0.67	42	0.0009
	MP [9]	0.43	0.43	0.45	0.46	0.48	0.49	0.50	0.51	0.54	0.55	5	0.0008
	PERT	**0.33**	**0.34**	**0.34**	**0.35**	**0.36**	**0.36**	**0.37**	**0.37**	**0.39**	**0.40**	**3**	**0.0011**
	Random	0.22	0.28	0.36	0.42	0.50	0.62	0.73	0.90	0.94	1.00	50	0.0001
	RISE [29]	0.12	0.12	0.23	0.32	0.42	0.52	0.6	0.88	0.88	0.92	73	0.0001
CricketX [24]	LEFTIST [12]	0.27	0.21	0.18	0.18	0.17	0.03	0.03	0.03	0.03	0.03	51	0.0001
	LIME [32]	0.13	0.18	0.22	0.25	0.28	0.30	0.33	0.36	0.40	0.47	33	0.0001
	SHAP [19]	0.23	0.33	0.37	0.40	0.42	0.43	0.44	0.45	0.47	0.48	34	0.0005
	MP [9]	0.07	0.09	0.09	0.13	0.15	0.16	0.17	0.19	0.19	0.23	2	0.0040
	PERT	**0.06**	**0.07**	**0.07**	**0.08**	**0.08**	**0.09**	**0.10**	**0.11**	**0.12**	**0.15**	**1**	**0.0048**

Table 4.5: Confidence-Suppression Metric performance for two key datasets with the RNN black-box model. Lower values are better for Saliency sum and Confidence suppression game, Higher values are better for saliency variance.

progressively *increasing* them during training. However, another option is *Backward Selection*, where saliency values are initially large and are *decreased* during training. Interestingly, the *Forward Selection* is significantly better than *Backward Selection*, indicating that carefully *adding* time steps produces a better ranking whilst preserving the fewest possible timesteps. Third, we experiment with five alternative time series replacement strategies to test the importance of the choice of replacement time series R's impact on black-box model f_c's prediction $P(C|\hat{X})$. Initially we consider an exhaustive search to find a single *best* (and *worst*) R from the background dataset $\mathcal{D}$. From this experiment, we notice that the AUC-Difference metric is sensitive to the choice of replacement time series R. However, by observing the relationship between the predicted confidence of f_c for instance-of-interest $\hat{X}$, $P(C|\hat{X})$ and for the perturbed instance X^*, $P(C|\hat{X}^*)$, we propose dual replacement sampling, where we sample a replacement time series from class-of-interest R_C and from opposing class R_O, and perform time step specific replacement which results in a substantial improvement in AUC-Difference metric, and when coupled with prioritization outperforms all other replacement strategies.

4.5.3 Hyperparameter Study

Producing explanations with PERT involves balancing the four key hyperparameters: The mean of Gaussian noise g_n and the $L_{\text{preservation}}$, L_{budget}, and L_{TV} coefficients.

We investigate the effects of tuning the coefficients of each in isolation in Figure 4.3 on Wafer dataset, keeping all unchanged parameters at their best-found values. As shown in Figure 4.3(a), we change the mean of the gaussian noise from -1 to 2 and notice that the optimal value lies between 0 and 1, indicating that a small amount of additive gaussian noise leads to the largest improvement in PERT's performance. This confirms the intuition behind the compared method MP [9], which employs a

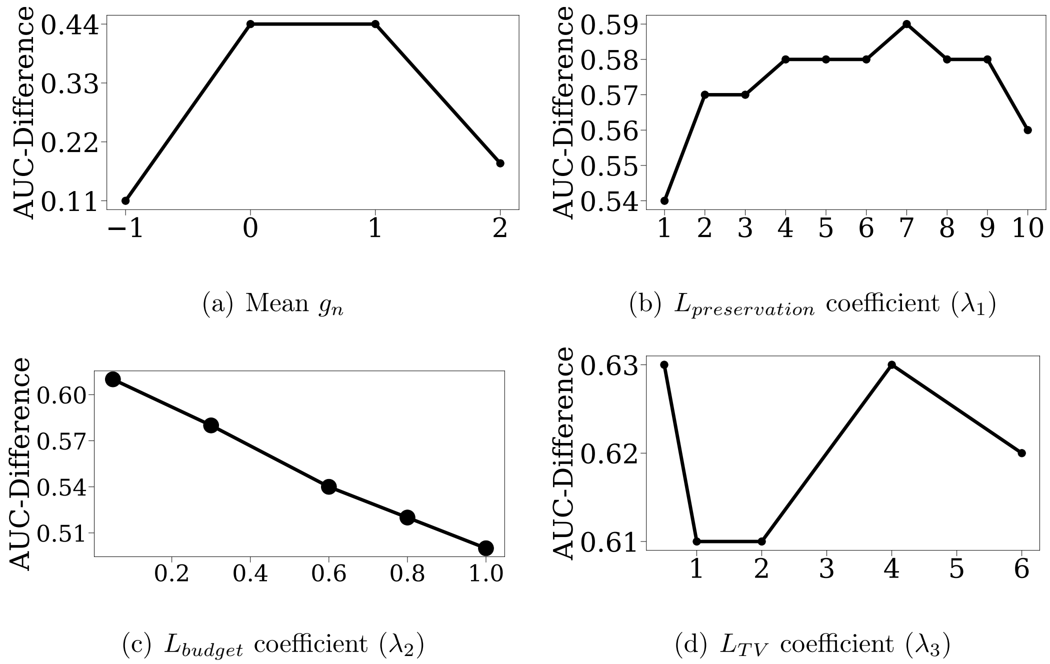

(a) Mean g_n

(b) $L_{preservation}$ coefficient (λ_1)

(c) L_{budget} coefficient (λ_2)

(d) L_{TV} coefficient (λ_3)

Figure 4.3: PERT Hyperparameter Study

similar strategy. Next, we find a non-linear trade-off for the $L_{\text{preservation}}$ coefficient: Too-low means not enough focus on producing good explanations, too-high begins to ignore the other crucial parts of the loss function, as shown in Figure 4.3(b). Third, as expected, a higher L_{budget} leads to lower AUC-Difference, as shown in Figure 4.3(c). This is because there is a trade-off between the L_{budget} and $L_{\text{preservation}}$, where the higher the coefficient on L_{TV} forces PERT to minimize the values of the saliency map during training, eventually ignoring the preservation task entirely. Finally, the results for the L_{TV} coefficient are shown in Figure 4.3(d), where we observe that the final AUC-Difference is quite robust to these changes in the coefficient, ranging only between 0.61 and 0.63. Compared methods use default hyperparameters.

4.5.4 Case Study

Blip dataset

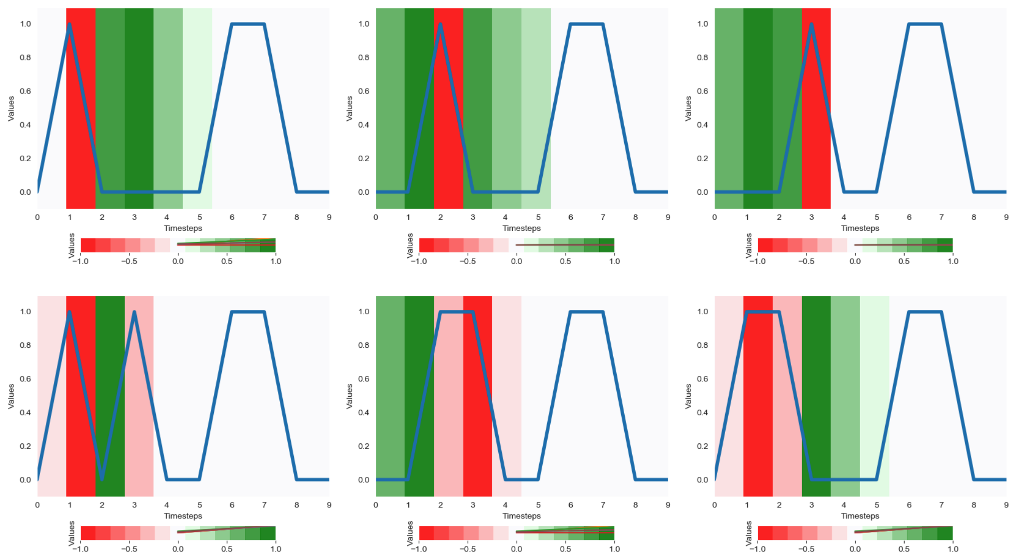

Figure 4.4: Blip Case Study.

The 10-timestep synthetic dataset is designed by choice in order to intuitively verify the explanation provided to showcase the black-box model's pattern identification capabilities. For class 0, there are 6 different variations of blip in the first five timesteps. For class 1, there exists a single pattern i.e, a single blip in the first five time steps. In order to test the black-box-model's capability to ignore certain common patterns, both the classes have a single blip in last 5 timesteps. In this dataset there is no well-defined ground-truth for which time steps are truly the most important. To overcome this limitation, we design a simple synthetic dataset, where some timesteps are essential to classification success, while some timesteps are entirely irrelevant. Specifically, we create a balanced dataset with two classes and a total of X training time series. Examples from the Negative class having ones are timesteps 2-4 and examples from the Positive class having any random combination of ones and zeros between timesteps 2 and 4. Timesteps six and seven are always ones and all other timesteps are always zeros. This way, to predict the class label of a time series, all a classifier needs to look at is timesteps two, three, and four.

CRICKETX dataset

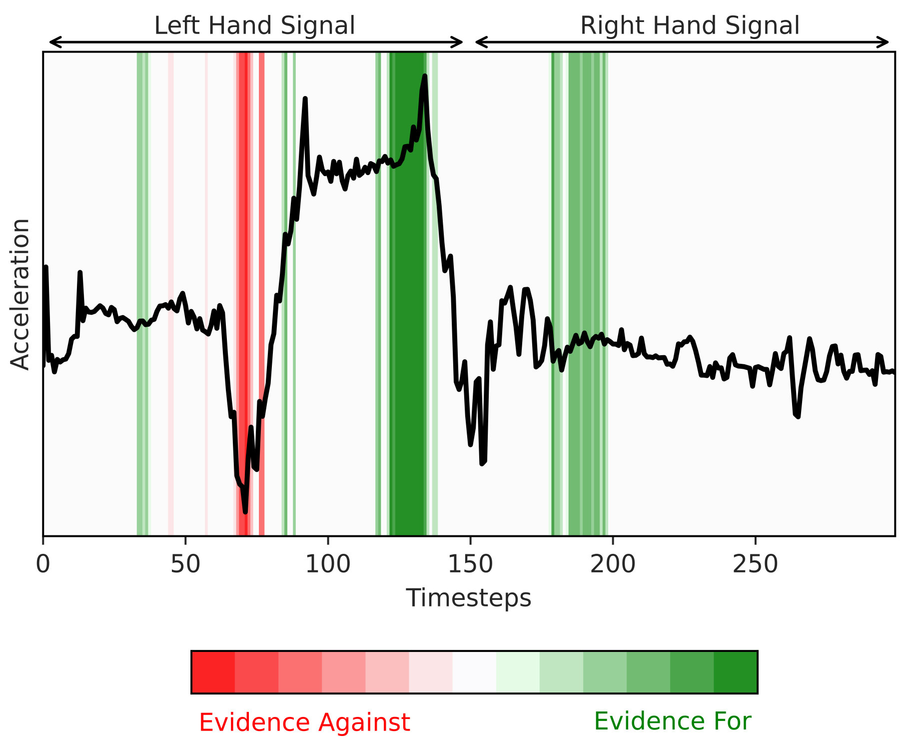

Figure 4.5: CRICKETX "No-Ball" Class Case Study
The signal is shown in black. Important time steps for the class-of-interest are shown in bright green and while bright red indicates important time steps for the opposing class.

CRICKETX dataset [24] contains length-300 time series and is a binary classification task: An umpire wearing a sensor on their wrists calls either *No Ball* or *Wide Ball* during a cricket match. The *No Ball* class has bursts of movement on the left side, indicating the umpire raised their left hand. The *Wide Ball* class has left-side *and* right-side bursts, indicating the umpire also raised their right hand. For this case study, we choose one instance from the *No Ball* class, which is known to be represented as as a spike in the left side of the time series. In Figure 4.5, we show the raw instance in black along with the saliency map produced by PERT colored according to the scale of the values in the saliency map. Intuitively, the brighter the colors, the more important the corresponding time series.

First, multiple bursts only on the left-side of the time series are an indication of strong evidence for the *No Ball* class, PERT accurately highlighted the highest burst in the brightest green region. Further, evidence for the *No Ball* class also appears on in the right-hand signal where there would have been a signal had it been *Wide Ball*. PERT's saliency map effectively highlights that the black-box classifier accurately used these important regions to predict *No Ball*. Additionally, this example gives us insight into the black-box model's prediction: The end of the left-hand signal (once the umpire's hand is raised and stabilized) is the strongest evidence supporting the model's decision. Second, bright red color bars indicate strong evidence for the opposite class had this been a *Wide Ball* (opposite class). This strongly indicates that the underlying model is using the information at these two regions far more than the others, exactly as expected for this example.

Chapter 5

Conclusion

In this work, we identify the need for attribution-based explanations for deep neural network-based time series classifiers. We then design PERT, a method that learns to highlight the timesteps that are most responsible and the degree to which they are important for the classifier's prediction. By adaptively *learning* a perturbation function, PERT creates explanations for input time series that are catered specifically to the dataset, time series instance, and individual timesteps, deriving evidence both *for* and *against* the model's prediction. This evidence, presented as one importance value per timestep, thus allows an end-user to understand what information their classifier was using during classification, increasing their trust in their model. In our experiments, we conclusively demonstrate that PERT accurately discovers the most-important timesteps as it outperforms five state-of-the-art alternatives on three key metrics on nine datasets.

Chapter 6

Future Work

6.1 Incorporating distance metrics

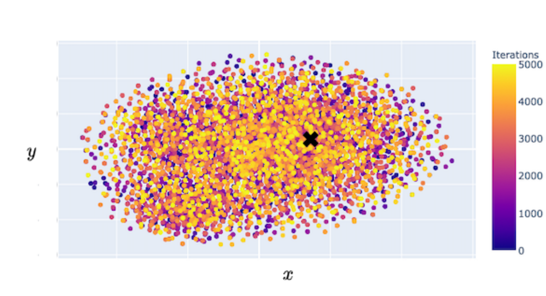

Figure 6.1: TSNE visualization of instance perturbations in LIME[32]

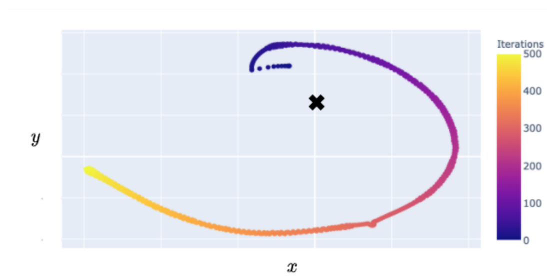

Figure 6.2: TSNE visualization of instance perturbations in PERT[9]

Figures 6.1 and 6.2 demonstrate the differences in the distances between random perturbations and learning to perturb methods. It is intriguing to understand the learning process behind the perturbations. In a few of the cases, the $L_{preservation}$ component of the loss function oscillates frequently suggesting a hypothesis - the specimen is very close to the class-decision boundary line. Such cases pave way for interesting ways of exploring the boundaries using distance metrics. To expand the boundary of our perturbations, the direction of expansion plays a crucial role i.e, whether to push the path of perturbation towards / away from the nearest opposing instance. Here are a few use cases of distance metrics. First, the use of distance metrics allows us to design a decay factor for the L_{budget} component based on the variance in the $L_{preservation}$ component (judging how close the perturbations are to the decision boundary). Second, we can enforce decay / increase of the distance between previous perturbation and the next perturbation based on the number of iterations leading to closer / farther perturbed instances. Third, the distance metric can be used to formulate an early stopping criterion. Finally, use of distance metrics might help reduce network artifacts induced by perturbations.

6.2 Extending to Multi-variate, Multi-class problems

PERT is designed to work with uni-variate binary classification problems. In contrast, the real-world problems are of multi-variate and multi-class types. To better adapt PERT for real-world problems, a few changes are necessary,

Prioritized Replacement Selector. A prioritized replacement selector is used to optimize the sampling of replacement time series from the background dataset. PERT makes use of two priority buffers, one for sampling instances from the same class (predicted class of instance $P(C|\hat{X})$) and the other for sampling instances from the opposing class. In a multi-class scenario, it is non-trivial to choose the opposing class due to the existence of > 2 classes. To support dual-sampling (same and opposing), we need a measure of distance between the instance of interest and respective classes. This translates to measuring the distance between a point p (instance of interest) and a distribution d (Class-specific distributions). We plan to make use of *Mahalanobis Distance* to support dual-sampling by deriving the opposing class for the given instance-of-interest.

Guided Perturbation Function. The function f_{gp} is responsible for learning to perturb the instance-of-interest. PERT uses θ, a one-dimensional parametric trainable vector to represent the saliency of each timestep for a uni-variate instance.

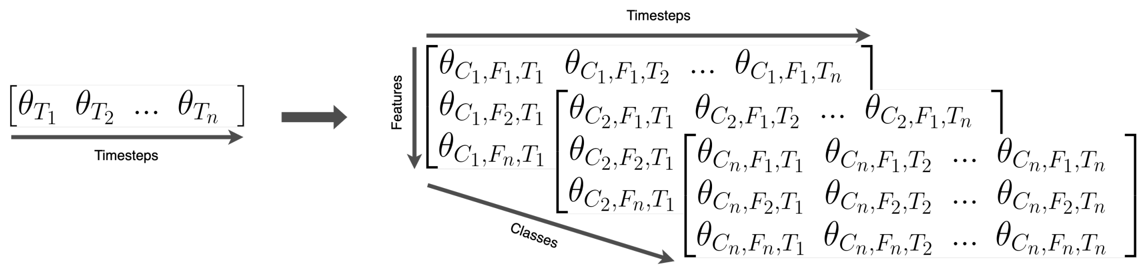

Figure 6.3: Learnable Multi-variate Multi-class Mask

Figure 6.3 showcases the necessary changes in the learnable mask θ of one dimension representing timesteps to a three dimension vector, where *classes*, *features* and *timesteps* are the dimensions of a multi-variate, multi-class setting.

Optimizing PERT. To derive instance-specific explanations, PERT uses *RMSE* function to preserve the class confidence of the instance-of-interest. However, the confidences are probabilistic measures and *RMSE* is not suited for probabilities, due to the presence of power operations. Probabilities, being fractions under 1, are significantly affected by the power operations (Square and Root). Calculating the squares of differences of probabilities, the values that are averaged are abnormally small, hence the model barely learns. This problem turns out to be exponentially challenging in a multi-class setting. To derive instance-specific explanations, it is crucial to preserve the probabilistic distribution of confidences predicted by the deep time series classifier. To best measure the similarity between two distributions, we plan to use Kullback-Liebler Divergence. KL Divergence is a measure of how one probability distribution is different from another probability distribution. $KL(P, Q)$ is the information gain/loss when distribution Q is used instead of distribution P.

6.3 Shared Saliencies

In a multi-class problem, there exists saliency maps explaining respective class confidences. In such cases, saliency maps of two or more different classes tend to be similar to each other suggesting the presence of shared saliencies. The presence of shared saliencies lead to an ambiguity in the derived evidences for the respective decision. Distinct class-specific saliency maps void of shared saliencies lead to intuitive (simple - few timesteps in the evidence and precise - unique evidence) explanations. To derive class-specific saliency maps, we subtract saliency maps of the other candidate classes from the saliency map of the target class.

$$\theta_t^* = \sum_{c \in candidates} P(c \mid \hat{X}) * max(\theta_t - \theta_c, 0)[c \neq t]$$

Bibliography

[1] Inès Arous, Ljiljana Dolamic, Jie Yang, Akansha Bhardwaj, Giuseppe Cuccu, and Philippe Cudré-Mauroux. Marta: Leveraging human rationales for explainable text classification. In *AAAI Conference on Artificial Intelligence*, 2021.

[2] S. Bach, Alexander Binder, Grégoire Montavon, F. Klauschen, K. Müller, and W. Samek. On pixel-wise explanations for non-linear classifier decisions by layer-wise relevance propagation. *PLoS ONE*, 10, 2015.

[3] J. Bento, P. Saleiro, F. Cruz, M. Figueiredo, and P. Bizarro. Timeshap: Explaining recurrent models through sequence perturbations. *ArXiv*, abs/2012.00073, 2020.

[4] Lukas Biewald. Experiment tracking with weights and biases, 2020. Software available from wandb.com.

[5] A. Charnes, B. Golany, M. Keane, and J. Rousseau. Extremal principle solutions of games in characteristic function form: Core, chebychev and shapley value generalizations. In *Econometrics of Planning and Efficiency*, pages 123–133. Springer Netherlands, Dordrecht, 1988.

[6] Yanping Chen, Eamonn Keogh, Bing Hu, Nurjahan Begum, Anthony Bagnall, Abdullah Mueen, and Gustavo Batista. The ucr time series classification archive, July 2015. `www.cs.ucr.edu/~eamonn/time_series_data/`.

[7] Eoin Delaney, Derek Greene, and Mark T. Keane. Instance-based counterfactual explanations for time series classification. *ArXiv*, abs/2009.13211, 2020.

[8] R. Fong, M. Patrick, and A. Vedaldi. Understanding deep networks via extremal perturbations and smooth masks. In *ICCV*, pages 2950–2958, 2019.

[9] R. Fong and A. Vedaldi. Interpretable explanations of black boxes by meaningful perturbation. *ICCV*, pages 3449–3457, 2017.

[10] Christopher Frye, Colin Rowat, and Ilya Feige. Asymmetric shapley values: incorporating causal knowledge into model-agnostic explainability. In H. Larochelle, M. Ranzato, R. Hadsell, M. F. Balcan, and H. Lin, editors, *Advances in Neural*

Information Processing Systems, volume 33, pages 1229–1239. Curran Associates, Inc., 2020.

[11] A. Goldberger, L. A. Amaral, L. Glass, Jeffrey M. Hausdorff, P. Ivanov, R. Mark, J. Mietus, G. Moody, C. Peng, and H. Stanley. Physiobank, physiotoolkit, and physionet: components of a new research resource for complex physiologic signals. *Circulation*, 101 23:E215–20, 2000.

[12] Maël Guillemé, V. Masson, Laurence Rozé, and A. Termier. Agnostic local explanation for time series classification. *ICTAI*, pages 432–439, 2019.

[13] Shenda Hong, Yuxi Zhou, Junyuan Shang, Cao Xiao, and Jimeng Sun. Opportunities and challenges in deep learning methods on electrocardiogram data: A systematic review. *Computers in biology and medicine*, 122:103801, 2020.

[14] A. A. Ismail, M. Gunady, H. Bravo, and S. Feizi. Benchmarking deep learning interpretability in time series predictions. *ArXiv*, abs/2010.13924, 2020.

[15] Aya Abdelsalam Ismail, Mohamed Gunady, Hector Corrada Bravo, and Soheil Feizi. Benchmarking deep learning interpretability in time series predictions. In H. Larochelle, M. Ranzato, R. Hadsell, M. F. Balcan, and H. Lin, editors, *Advances in Neural Information Processing Systems*, volume 33, pages 6441–6452. Curran Associates, Inc., 2020.

[16] Deepak A Kaji, John R Zech, Jun S Kim, Samuel K Cho, Neha S Dangayach, Anthony B Costa, and Eric K Oermann. An attention based deep learning model of clinical events in the intensive care unit. *PloS one*, 14(2):e0211057, 2019.

[17] Diederik P. Kingma and Jimmy Ba. Adam: A method for stochastic optimization. *CoRR*, abs/1412.6980, 2015.

[18] Sawan Kumar and P. Talukdar. Nile : Natural language inference with faithful natural language explanations. In *ACL*, 2020.

[19] Scott L. and Su-In L. A unified approach to interpreting model predictions. *Advances in Neural Information Processing Systems 30*, pages 4765–4774, 2017.

[20] Tao Lei, R. Barzilay, and T. Jaakkola. Rationalizing neural predictions. In *EMNLP*, 2016.

[21] Scott M Lundberg and Su-In Lee. A unified approach to interpreting model predictions. In I. Guyon, U. V. Luxburg, S. Bengio, H. Wallach, R. Fergus, S. Vishwanathan, and R. Garnett, editors, *Advances in Neural Information Processing Systems 30*, pages 4765–4774. Curran Associates, Inc., 2017.

[22] L. V. D. Maaten and Geoffrey E. Hinton. Visualizing data using t-sne. *Journal of Machine Learning Research*, 9:2579–2605, 2008.

[23] V. Mnih, K. Kavukcuoglu, D. Silver, A. Graves, Ioannis Antonoglou, Daan Wierstra, and Martin A. Riedmiller. Playing atari with deep reinforcement learning. *ArXiv*, abs/1312.5602, 2013.

[24] A. Mueen, E.J. Keogh, and N E. Young. Logical-shapelets: an expressive primitive for time series classification. In *KDD*, pages 1154–1162, 2011.

[25] F. Mujkanovic, V. Doskoč, M. Schirneck, P. Schäfer, and T. Friedrich. timexplain–a framework for explaining the predictions of time series classifiers. *ArXiv*, abs/2007.07606, 2020.

[26] Felix Mujkanovic, Vanja Doskoc, Martin Schirneck, P. Schäfer, and T. Friedrich. timexplain - a framework for explaining the predictions of time series classifiers. *ArXiv*, abs/2007.07606, 2020.

[27] R. Olszewski, R. Maxion, and D. Siewiorek. Generalized feature extraction for structural pattern recognition in time-series data. *PhD thesis*, 2001.

[28] Adam Paszke, Sam Gross, Francisco Massa, Adam Lerer, James Bradbury, Gregory Chanan, Trevor Killeen, Zeming Lin, Natalia Gimelshein, Luca Antiga, Alban Desmaison, Andreas Kopf, Edward Yang, Zachary DeVito, Martin Raison, Alykhan Tejani, Sasank Chilamkurthy, Benoit Steiner, Lu Fang, Junjie Bai, and Soumith Chintala. Pytorch: An imperative style, high-performance deep learning library. In H. Wallach, H. Larochelle, A. Beygelzimer, F. d'Alché-Buc, E. Fox, and R. Garnett, editors, *Advances in Neural Information Processing Systems 32*, pages 8024–8035. Curran Associates, Inc., 2019.

[29] Vitali Petsiuk, Abir Das, and Kate Saenko. Rise: Randomized input sampling for explanation of black-box models. *CoRR*, abs/1806.07421, 2018.

[30] C. Ratanamahatana and Eamonn J. Keogh. Three myths about dynamic time warping data mining. In *SDM*, pages 506–510. SIAM, 2005.

[31] A. Ribeiro, M. Ribeiro, G. Paixão, D. Oliveira, P. Gomes, A. Canazart, P. Ferreira, C. Andersson, P. Macfarlane, and et al. Automatic diagnosis of the 12-lead ecg using a deep neural network. *Nature Communications*, 11(1), Apr 2020.

[32] Marco Tulio Ribeiro, Sameer Singh, and Carlos Guestrin. "why should i trust you?": Explaining the predictions of any classifier. *CoRR*, abs/1602.04938, 2016.

[33] Udo S., Hiba A., Mennatallah E., Daniela O., and Daniel A.K. Towards a rigorous evaluation of xai methods on time series. *CoRR*, abs/1909.07082, 2019.

[34] Udo S., Daniela O., Daniel A.K., and Mennatallah E. An empirical study of explainable ai techniques on deep learning models for time series tasks. *ArXiv*, abs/2012.04344.

[35] T. Schaul, John Quan, Ioannis Antonoglou, and D. Silver. Prioritized experience replay. *CoRR*, abs/1511.05952, 2016.

[36] R. R. Selvaraju, Abhishek Das, Ramakrishna Vedantam, Michael Cogswell, D. Parikh, and Dhruv Batra. Grad-cam: Why did you say that? visual explanations from deep networks via gradient-based localization. 2016.

[37] Cansu Sen, Thomas Hartvigsen, Biao Yin, Xiangnan Kong, and Elke Rundensteiner. Human attention maps for text classification: Do humans and neural networks focus on the same words? In *Proceedings of the 58th Annual Meeting of the Association for Computational Linguistics*, 2020.

[38] Avanti Shrikumar, Peyton Greenside, and Anshul Kundaje. Learning important features through propagating activation differences. In *International Conference on Machine Learning*, pages 3145–3153, 2017.

[39] K. Simonyan, A. Vedaldi, and Andrew Zisserman. Deep inside convolutional networks: Visualising image classification models and saliency maps. *CoRR*, abs/1312.6034, 2014.

[40] Karen Simonyan, Andrea Vedaldi, and Andrew Zisserman. Deep inside convolutional networks: Visualising image classification models and saliency maps. *arXiv preprint arXiv:1312.6034*, 2013.

[41] H. Song, D. Rajan, J. Thiagarajan, and A. Spanias. Attend and diagnose: Clinical time series analysis using attention models. In *32nd AAAI Conference on Artificial Intelligence, AAAI 2018*, pages 4091–4098. AAAI press, 2018.

[42] Jost Tobias Springenberg, A. Dosovitskiy, T. Brox, and Martin A. Riedmiller. Striving for simplicity: The all convolutional net. *CoRR*, abs/1412.6806, 2015.

[43] Mukund Sundararajan, Ankur Taly, and Qiqi Yan. Axiomatic attribution for deep networks. In *Proceedings of the 34th International Conference on Machine Learning-Volume 70*, pages 3319–3328, 2017.

[44] Sana Tonekaboni, Shalmali Joshi, David Duvenaud, and Anna Goldenberg. What went wrong and when? instance-wise feature importance for time-series models. *Advances in Neural Information Processing Systems*, 2020.

[45] Yanbo Xu, Siddharth Biswal, Shriprasad R Deshpande, Kevin O Maher, and Jimeng Sun. Raim: Recurrent attentive and intensive model of multimodal patient monitoring data. In *Proceedings of the 24th ACM SIGKDD international conference on Knowledge Discovery & Data Mining*, pages 2565–2573, 2018.

[46] Lexiang Ye and Eamonn Keogh. Time series shapelets: a new primitive for data mining. In *SIGKDD International Conference on Knowledge Discovery and Data Mining*, pages 947–956. ACM, 2009.

[47] M. Zeiler and R. Fergus. Visualizing and understanding convolutional networks. In *European conference on computer vision*, pages 818–833. Springer, 2014.

[48] Matthew D. Zeiler and R. Fergus. Visualizing and understanding convolutional networks. *ArXiv*, abs/1311.2901, 2014.

[49] J. Zhang, Zhe Lin, Jonathan Brandt, Xiaohui Shen, and S. Sclaroff. Top-down neural attention by excitation backprop. *International Journal of Computer Vision*, 126:1084–1102, 2017.

[50] B. Zhou, A. Khosla, Àgata Lapedriza, A. Oliva, and A. Torralba. Learning deep features for discriminative localization. *2016 IEEE Conference on Computer Vision and Pattern Recognition (CVPR)*, pages 2921–2929, 2016.